APPLIED SCIENCES AND ENGINEERING

Increasing bulk photovoltaic current by strain tuning

Shankari Nadupalli[1], Jens Kreisel[1,2], Torsten Granzow[1]*

Photovoltaic phenomena are widely exploited not only for primary energy generation but also in photocatalytic, photoelectrochemistry, or optoelectronic applications. In contrast to the interface-based photovoltaic effect of semiconductors, the anomalous or bulk photovoltaic effect in ferroelectrics is not bound by the Shockley-Queisser limit and, thus, can potentially reach high efficiencies. Here, we observe in the example of an Fe-doped $LiNbO_3$ bulk single crystal the existence of a purely intrinsic "piezophotovoltaic" effect that leads to a linear increase in photovoltaic current density. The increase reaches 75% under a low uniaxial compressive stress of 10 MPa, corresponding to a strain of only 0.005%. The physical origin and symmetry properties of the effect are investigated, and its potential for strain-tuned efficiency increase in nonconventional photovoltaic materials is presented.

INTRODUCTION: PHOTOFERROELECTRICS, FLEXOPHOTOVOLTAIC, AND PIEZOPHOTOVOLTAIC EFFECT

With the discovery of photovoltaic (PV) energy conversion efficiencies up to 10% in domain-engineered $BiFeO_3$ ferroelectric films under above-bandgap illumination (1, 2), research in photoferroelectric phenomena has strongly intensified (3, 4). Because of their polar structure, ferroelectrics display unconventional PV phenomena such as the bulk PV effect (BPVE) (5, 6). The BPVE does not rely on any interface such as a p-n junction, is not bound by the Shockley-Queisser limit, and therefore has the potential to drastically increase conversion efficiencies of solar cells (7), particularly when combined with bandgap tuning of the ferroelectric (8). Charge separation can be increased by ferroelectric domain walls, either through their electric potential (2, 9, 10) or through their increased carrier mobility (11, 12). Mechanical boundary conditions play an important role for the PV effect in highly strained ferroelectric films (13, 14). In this context, Yang et al. (15) recently found a BPVE in nonpolar materials under a strain gradient. As the inhomogeneous strain provides the symmetry breaking essential for bulk PV phenomena, they called this effect "flexo-PV," in analogy to the "flexoelectric" effect.

Flexoelectricity creates electric polarization in any material under a stress gradient, just as piezoelectricity creates or changes polarization under homogeneous stress in a piezo- or ferroelectric material, respectively (16). Likewise, the flexo-PV effect creates a bulk PV response in a nonpolar material under a stress/strain gradient. Still, there is no report on an analogous intrinsic "piezo-PV" (PPV) effect that creates or changes the BPVE of noncentrosymmetric or ferroelectric materials under homogeneous stress. This PPV effect could outperform the flexo-PV effect in photoelectric applications, just as piezoelectricity is typically more efficient than flexoelectricity in strain sensing or energy harvesting. It has to be noted that an intrinsic PPV effect would be fundamentally different from extrinsic effects such as the so-called piezophototronic effect that relies on a change of the Schottky barrier height due to piezoelectric charges (17).

Here, we provide evidence for a purely intrinsic PPV effect in Fe-doped $LiNbO_3$ (LN:Fe), a prototypical bulk PV material (18). It is quantified by a PPV tensor and leads to an increase in the bulk PV current by

as much as 75% under a homogeneous uniaxial compressive stress of only 10 MPa. At a modulus of 200 GPa, this corresponds to a strain of just 0.005%; much larger effects can be expected in thin films, where strains on the order of 1% can be achieved (19). The effect is distinguished from the piezophototronic effect. On the basis of the wavelength dependence and symmetry properties of this new effect and a model of ballistic charge transport (20) and polaron hopping (21), it is suggested to arise from an increase in charge carrier mobility.

RESULTS

Direct measurements of bulk PV current density

A monodomain crystal of $LiNbO_3$ doped with 0.03 mole percent (mol %) Fe is homogeneously illuminated with linearly polarized light of wavelength λ at an intensity I under short-circuit conditions, as shown in Fig. 1A. The orientation of the coordinate system in relation to the sample edges and crystallographic structure is schematically depicted in Fig. 1 (B and C). The 3-direction coincides with the polar crystallographic c axis, the 2-direction is the crystallographic a axis, and the 1-direction forms a right-handed Cartesian coordinate system with the other two. The Fe dopant ions are incorporated on the Li site, forming $Fe_{Li}^{2+/3+}$ defects.

Figure 2A exemplarily depicts the short-circuit current density j_3^{sc} when extraordinarily polarized light with wavelength λ = 532 nm and intensity $I = 98$ W m^{-2} is switched on and off. At the start and stop of the illumination, there are brief pyroelectric pulses before j_3^{sc} stabilizes. In general, the steady-state BPVE is described by the third-rank bulk PV tensor β, relating the short-circuit current density j^{sc} with the components of the electric field of the incident light E: $j_i^{sc} = (1/2)\beta_{ijk}(E_j^* E_k + E_j E_k^*)$. Here, the "*" denotes the complex conjugate (22, 23). In Fig. 2B, the measured intensity dependence of j_3^{sc} is displayed for excitation wavelengths of λ = 450, 473, and 532 nm, corresponding to photon energies of 2.76, 2.62, and 2.33 eV, respectively. As expected, j_3^{sc} is proportional to I; the slope gives the wavelength-dependent component β_{333} of the bulk PV tensor. Other components β_{ijj} with identical second and third index can be measured by changing the crystal orientation and light polarization. For symmetry reasons, only β_{333}, $\beta_{311} = \beta_{322}$, and $\beta_{222} = -\beta_{211}$ have nonzero values. The measured values of all components are comparable to those reported in literature under similar measurement conditions (24). To correlate the BPVE with the optical absorption, the inset of Fig. 2B shows the absorption coefficient α of the Fe-doped crystal measured in transmission for 300 nm ≤ λ ≤ 600 nm, contrasted with that of undoped $LiNbO_3$. The doped sample is transparent

[1]Materials Research and Technology Department, Luxembourg Institute of Science and Technology, 41 Rue du Brill, L-4422 Belvaux, Luxembourg. [2]Physics and Materials Science Research Unit, University of Luxembourg, 41 Rue du Brill, 4422 Belvaux, Luxembourg.
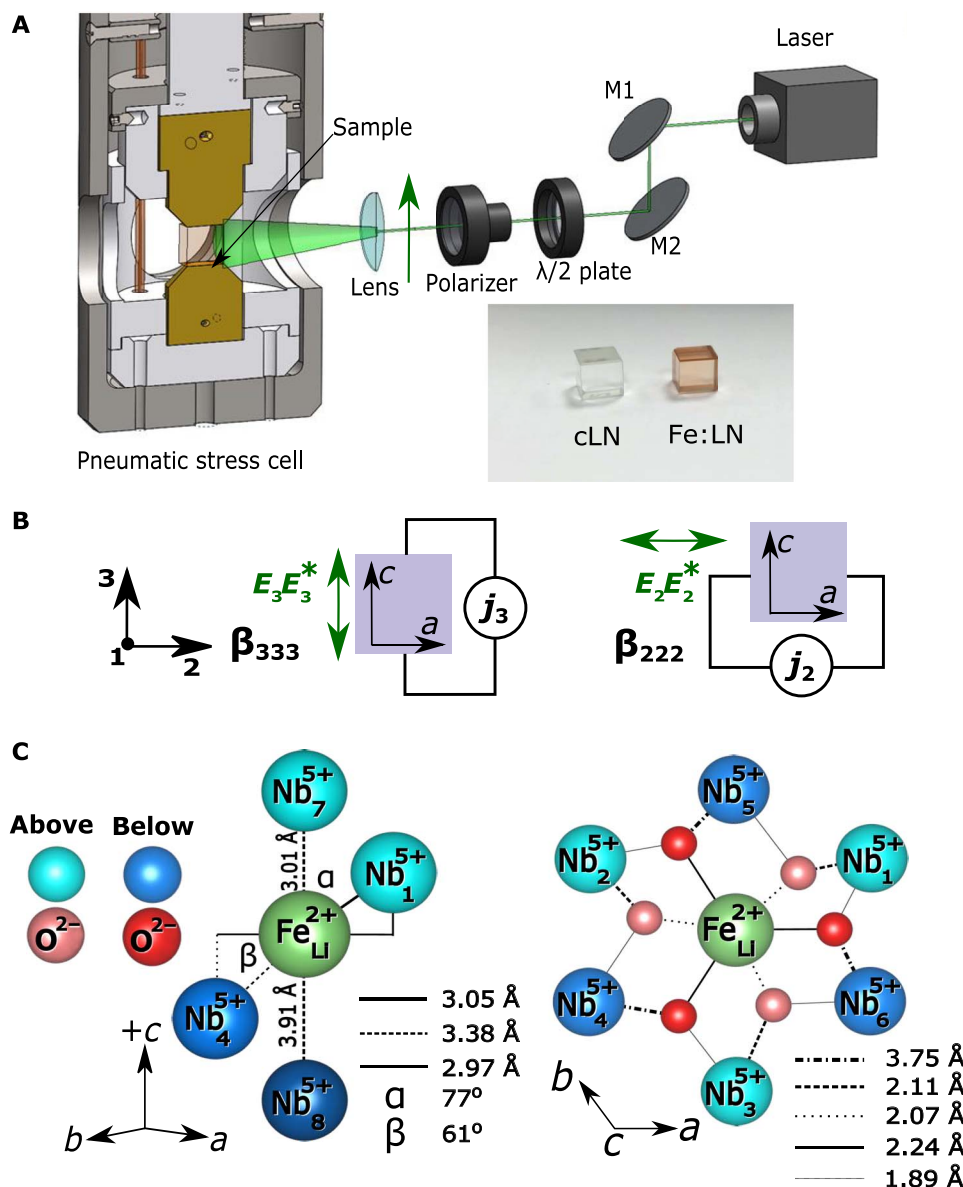*Corresponding author. Email: torsten.granzow@list.lu

Fig. 1. Measurement setup and crystal structure. (**A**) Setup for bulk PV current measurement with a crosscut of the pressure cell. The lower part shows a photograph of the doped sample and an undoped LiNbO$_3$ crystal for comparison. (**B**) Orientation of the coordinate system with respect to the crystallographic axes. (**C**) Structure of LiNbO$_3$ with interatomic distances. Left: View perpendicular to the polar axis (with all O^{2-} omitted). Right: View along the polar axis (with some O^{2-} omitted). Crystallographic data are taken from (21).

at high wavelengths, there is an absorption peak of the Fe donor centers around λ = 460 nm, and α increases strongly as the bandgap of 3.15 eV, corresponding to a wavelength of λ = 395 nm, is approached.

To facilitate the analysis of the physical processes for bulk PV charge transport, it is often described using the Glass coefficients $G_{ijk} = \beta_{ijk}/\alpha$ (5, 25). Here, we observe values of $G_{333} = 32 \times 10^{-12}$, 35×10^{-12}, and 51×10^{-12} Am W^{-1} for λ = 532, 473, and 450 nm, respectively. G_{333} is nearly identical for the two longer wavelengths. This indicates that the bulk PV charge transport is based on the same mechanism of photoexcitation exclusively from the Fe^{2+} donor centers. At the shortest wavelength, corresponding to the highest excitation energy, G_{333} is notably larger. Here, band-band transitions start to become relevant for the bulk PV charge transport.

Stress dependence of bulk PV current

Applying a uniaxial compressive stress σ$_{33}$ to the sample notably increases the saturation value of the short-circuit current, as documented in Fig. 2A. The development of β$_{333}$ with stress σ$_{33}$ is displayed in Fig. 3A for three excitation wavelengths, showing a linear increase at all wavelengths. It is thus possible to quantify the effect by a fifth-rank tensor γ, defined by the equation β$_{ijk}$ = β$_{ijk}$ (σ = 0) + γ$_{ijklm}$σ$_{lm}$ and referred to as PPV tensor in the following. The meaning of the indices of γ is visualized in Fig. 3B: The first index, i, denotes the direction of the current; the second and third indices, j and k, respectively, refer to the orientation of the light polarization, and the fourth and fifth indices, l and m, respectively, indicate the direction of stress. For uniaxial stress, symmetry considerations predict 38 nonzero components of γ, of which 13 are independent.
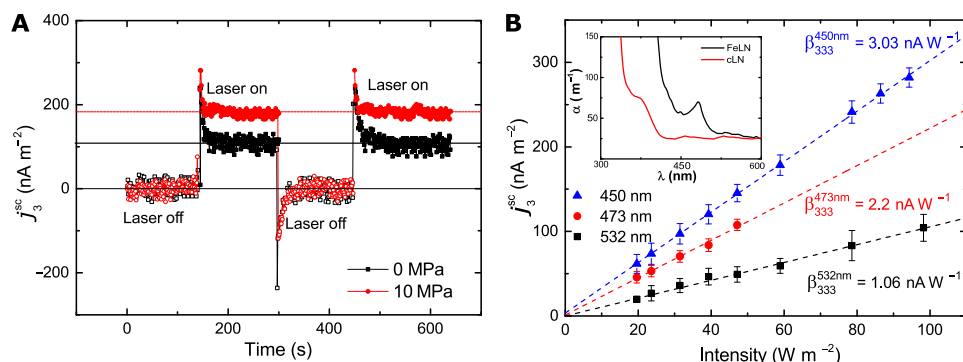
Fig. 2. BPVE in LN:Fe. (**A**) Current density j_3^{sc} of LN:Fe (0.03 mol %) as a function of time, switching on/off light polarized in the 3-direction with wavelength $\lambda = 532$ nm and intensity $I = 98$ W m^{-2} with/without compressive stress $\sigma_{33} = 10$ MPa. (**B**) Zero stress j_3^{sc} as function of I for three different λ values. The slope defines the component β_{333} of the bulk PV tensor. The inset shows absorption spectra of LN:Fe and undoped LiNbO$_3$. The Fe absorption band around $\lambda = 460$ nm is visible for the doped sample.

It can be seen in Fig. 3A that while the highest zero-stress value of $\beta_{333} = 3.03$ nA W^{-1} is observed at $\lambda = 450$ nm, the susceptibility to stress is highest at $\lambda = 532$ nm. Here, the value is $\gamma_{33333} = 78$ nA W^{-1} GPa^{-1}, leading to an increase in the PV short-circuit current by nearly 75% under a stress of 10 MPa.

To test the symmetry properties of the PPV effect, the stress dependence of β_{233} is of particular interest. It is shown at $\lambda = 532$ nm in Fig. 3C, with mechanical stress applied parallel and perpendicular to the polar axis, i.e., under σ_{33} and σ_{22}, respectively. Without stress, β_{233} should be zero for symmetry reasons, yet a finite value of 0.139 nA W^{-1} is observed at zero stress. It is most likely due to a photocurrent driven by the interface between the metal electrode and the crystal. β_{233} remains unchanged under σ_{33} within the measurement error, and γ_{23333} is nonzero only because of statistical effects in the linear fit. β_{233} increases drastically under σ_{22}. Because of the low zero-stress value, the relative increase reaches more than 500% at 10 MPa. The reason lies in the symmetry of the arrangement. A schematic representation of the stress with respect to the crystal structure is shown in Fig. 3D: σ_{33} parallel to the polar axis leaves the symmetry of the system unchanged. It remains in the point group 3m of the LiNbO$_3$ crystal structure. In contrast, σ_{22} perpendicular to the polar axis breaks the symmetry, lowering it to the monoclinic point group m in which a nonzero β_{233} exists.

It could be argued that the observed changes in the PV short-circuit current are not an intrinsic property of the crystal but an interface effect: As the sample is piezoelectric, putting it under stress can generate charges at the electroded interfaces, which, in turn, will modify the Schottky barrier and, thereby, the photocurrent. This coupling between piezoelectricity and semiconductor properties is known as the "piezotronic" effect or, when photoexcited electrons are added to the picture, the piezophototronic effect (*17, 26*). This interplay between piezoelectric and PV properties has been described before (*27, 28*). However, in the present case, the measurements did not show a systematic dependence on the electrode material, which should be expected if the effect was based on a variation of Schottky barrier height. To further test the potential influence of piezoelectric surface charges, Fig. 3E compares two pairs of PPV tensor components: the pair $\gamma_{33333} = 78$ nA W^{-1} GPa^{-1} and $\gamma_{32233} = 19$ nA W^{-1} GPa^{-1} with the pair $\gamma_{23322} = 53$ nA W^{-1} GPa^{-1} and $\gamma_{22222} = 5.3$ nA W^{-1} GPa^{-1}. Within each pair, only the direction of light polarization changes. The first pair is measured under stress in the 3-direction, so any piezoelectric response can be based only on the piezoelectric coefficient $d_{333} \approx 6.0$ pC/N. For the second pair, the stress is in the 2-direction. A piezoelectric response would be based on $d_{222} \approx 20.8$ pC/N. Consequently, if the PPV effect depended on piezoelectricity,

then γ should be approximately equal within each pair, and it should be substantially larger for the second pair than for the first pair. This is shown in Fig. 3F, which schematically depicts the development of the barrier height for both stress conditions. Since this is not the case, the PPV effect is an intrinsic bulk phenomenon and distinguished from the interface-based piezotronic or piezophototronic effect.

To make sure that the observed effects were not specific to one type of crystal or one wavelength, the main components of γ_{ijjkk} were additionally measured in LiNbO$_3$ doped with 0.1 mol % Fe at $\lambda = 450, 473$, and 532 nm, i.e., the three wavelengths already used for the measurements in Figs. 2B and 3A. These measurements support the results presented above (see the Supplementary Materials).

DISCUSSION
Origin of bulk PV current
The PPV behavior can be explained on the basis of a charge transport model proposed by Schirmer et al. (*21*). It emphasizes the critical role played by polarons in LiNbO$_3$: Illumination in the blue-green range photoexcites electrons in LN:Fe from an Fe$_{Li}^{2+}$ donor center into a Nb$_{Nb}^{4+}$ large polaronic state (*29, 30*). The excitation probability from the Fe$_{Li}^{2+}$ to each of the eight surrounding Nb$_{Nb}^{5+}$ ions depends on the interatomic distances (*21*), which are not equal due to the polar structure of the ferroelectric as depicted in Fig. 1C. Using the notation of Fig. 1C, more electrons are excited to the Nb$_7$ (i.e., along the direction of the polar axis) than to the Nb$_8$ (i.e., antiparallel to the polar axis); similar statements can be made for the other Nb positions. The asymmetry in the excitation direction is the basis for the observed macroscopic net current. Once excited and before thermalization, which typically happens within 10^{-13}s (*31*), the polarons travel in the direction of excitation by ballistic hopping. After thermalization, the electrons continue to move by thermally activated hopping, but this undirected movement does not constructively contribute to macroscopic charge transport. The BPVE in LiNbO$_3$ is, thus, not a consequence of the existence of a spontaneous polarization but arises directly from the noncentrosymmetric structure.

Influence of stress
Two aspects of the charge transport can be influenced by stress: the initial excitation step and the subsequent nonthermalized hopping. It is unlikely that changes in the initial excitation play an important role: Measurements of the absorption coefficient under stress revealed an increase of only about 1% under 10 MPa at $\lambda = 532$ nm (see the Supplementary Materials). The number of photoexcited charge carriers
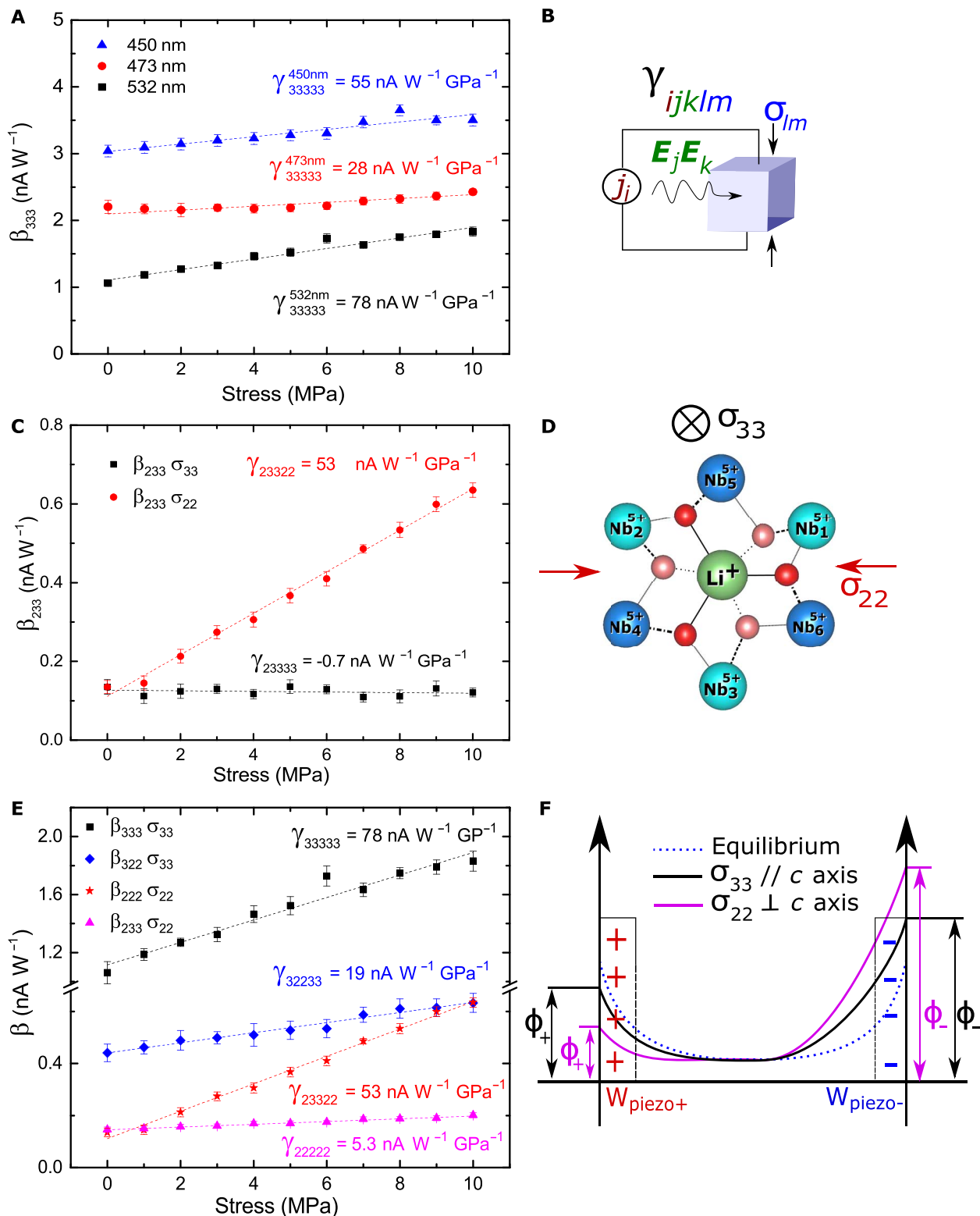
Fig. 3. Properties of the PPV effect. (**A**) Development of β_{333} with stress σ_{33} at three wavelengths. The slope defines the PPV tensor element γ_{33333}. (**B**) Definition of γ_{ijklm}: Index i denotes current direction, j and k denote light polarization, and l and m denote stress direction. (**C**) β_{233} under stress σ_{33} and σ_{22}, defining γ_{23333} and γ_{23322}, respectively. (**D**) Symmetry under stress: σ_{33} along the polar axis does not change the symmetry (point group $3m$), and σ_{22} perpendicular to the polar axis lowers the symmetry to point group m. (**E**) Comparison of two pairs of components of the PPV tensor. γ_{33333} and γ_{32233} differ only in light polarization direction, as does the pair γ_{23322} and γ_{22222}. (**F**) The piezotronic change of energy barriers at the metal electrodes is larger for σ_{22} owing to the larger piezoelectric coefficient d_{222}.

therefore does not change notably with stress and cannot account for the large increase in current. In addition, the asymmetry that is the basis for the BPVE is decreased under a compressive stress σ_{33}, which should result in negative values for γ. This is not observed. Therefore, it is reasonable to ascribe the PPV effect to increased nonthermalized polaron hopping. The energy of phonons involved in polaron formation decreases under stress, making hopping between neighboring Nb sites easier.

The findings prove the existence of an intrinsic PPV effect that can drastically increase light-induced current by about 75% even at moderate stress levels of 10 MPa. As the elastic modulus of $LiNbO_3$ is around 200 GPa, this corresponds to a strain of about 50 parts per million. It is difficult to achieve much higher strain in macroscopic samples, but in a thin film, a strain that is higher by several orders of magnitude can be easily generated (19). It is, of course, difficult to extrapolate the results presented here to such high levels of strain, but the PPV effect holds promise to substantially increase PV charge transport in thin-film applications as well. The basic material need not even have bulk PV properties: As demonstrated in Fig. 3 (C and D), a homogeneous stress can reduce the symmetry of the system to create finite values for a bulk PV tensor component that, without stress, vanishes for symmetry reasons. The search for efficient bulk PV charge transport is thus no more limited to pyro- or ferroelectric materials but can be extended to any noncentrosymmetric structure. In addition, higher conversion efficiencies have been predicted by Young et al. (32) for $LiNbO_3$-like structures with a smaller bandgap. Following this path of materials design further may open a path to PV energy generation with efficiencies surpassing the Shockley-Queisser limit even at longer light wavelengths.

MATERIALS AND METHODS
The main measurements were performed using Czochralski-grown $LiNbO_3$ single crystals doped with 0.03 mol % Fe (Deltronic Crystal Industries, Dover, NJ, USA), with supporting measurements on samples doped with 0.1 mol % Fe from the same source. The samples were cubes with an edge length of 10 mm, with one edge parallel to the crystallographic c direction, i.e., the polar axis, and one edge parallel to the crystallographic a direction. For the measurements of the short-circuit current, a pneumatic stress cell capable of providing a compressive load of up to 8 kN and allowing illumination of the sample in the direction perpendicular to the uniaxial compressive stress was used. A schematic of the setup and the samples are depicted in Fig. 1A. To check the homogeneity of the stress state in the crystal, a finite element model of the sample was created (see the Supplementary Materials). It showed that stress distribution in the sample does not deviate more than 5% from the expected value in more than 95% of the sample volume.

When the current was measured in the direction parallel to the stress, the brass dies of the cell acted as electrodes. For current measurements perpendicular to the stress direction, silver paint electrodes were applied to the nonilluminated crystal faces. Other electrode materials such as sputtered gold or platinum were also investigated; it was observed that the choice of electrode material did not influence the observed effects. Current was measured using a Keithley 6514 electrometer. Illumination was achieved using diode lasers (Changchun New Industries Optoelectronics Technology Co., PR China) with wavelengths of 450, 473, and 532 nm, corresponding to photon energies of 2.76, 2.62, and 2.33 eV, respectively. Light intensity and polarization direction were controlled using a half–wave plate and a Glan-Thompson polarizer,

and beam expansion was achieved by concave lenses (Thorlabs GmbH, Dachau, Germany). Absorption spectra were measured on a Lambda 950 UV/Vis/IR spectrometer (PerkinElmer, Zaventem, Belgium).

SUPPLEMENTARY MATERIALS
Supplementary material for this article is available at http://advances.sciencemag.org/cgi/content/full/5/3/eaau9199/DC1
Supplementary Text
Fig. S1. PPV tensor components in LN:Fe (0.03 mol %).
Fig. S2. PPV tensor components in LN:Fe (0.1 mol %).
Fig. S3. Stress distribution under uniaxial load.
Fig. S4. Stress dependence of absorption and bulk PV increase.

REFERENCES AND NOTES
1. S. Y. Yang, J. Seidel, S. J. Byrnes, P. Shafer, C.-H. Yang, M. D. Rossell, P. Yu, Y.-H. Chu, J. F. Scott, J. W. Ager III, L. W. Martin, R. Ramesh, Above-bandgap voltages from ferroelectric photovoltaic devices. Nat. Nanotechnol. 5, 143–147 (2010).
2. J. Seidel, D. Fu, S.-Y. Yang, E. Alarcón-Lladó, J. Wu, R. Ramesh, J. W. Ager III, Efficient photovoltaic current generation at ferroelectric domain walls. Phys. Rev. Lett. 107, 126805 (2011).
3. J. Kreisel, M. Alexe, P. A. Thomas, A photoferroelectric material is more than the sum of its parts. Nat. Mater. 11, 260 (2012).
4. C. Paillard, X. Bai, I. C. Infante, M. Guennou, G. Geneste, M. Alexe, J. Kreisel, B. Dkhil, Photovoltaics with ferroelectrics: Current status and beyond. Adv. Mater. 28, 5153–5168 (2016).
5. A. M. Glass, D. von der Linde, T. J. Negran, High-voltage bulk photovoltaic effect and the photorefractive process in $LiNbO_3$. Appl. Phys. Lett. 25, 233–235 (1974).
6. A. M. Glass, D. von der Linde, D. H. Auston, T. J. Negran, Excited-state polarization, bulk photovoltaic effect and the photorefractive effect in electrically polarized media. J. Electron. Mater. 4, 915–943 (1975).
7. J. E. Spanier, V. M. Fridkin, A. M. Rappe, A. R. Akbashev, A. Polemi, Y. Qi, Z. Gu, S. M. Young, C. J. Hawley, D. Imbrenda, G. Xiao, A. L. Bennett-Jackson, C. L. Johnson, Power conversion efficiency exceeding the Shockley–Queisser limit in a ferroelectric insulator. Nat. Photonics 10, 611–616 (2016).
8. R. Nechache, C. Harnagea, S. Li, L. Cardenas, W. Huang, J. Chakrabartty, F. Rosei, Bandgap tuning of multiferroic oxide solar cells. Nat. Photonics 9, 61–67 (2015).
9. R. Inoue, S. Ishikawa, R. Imura, Y. Kitanaka, T. Oguchi, Y. Noguchi, M. Miyayama, Giant photovoltaic effect of ferroelectric domain walls in perovskite single crystals. Sci. Rep. 5, 14741 (2015).
10. H. Matsuo, Y. Kitanaka, R. Inoue, Y. Noguchi, M. Miyayama, T. Kiguchi, T. J. Konno, Bulk and domain-wall effects in ferroelectric photovoltaics. Phys. Rev. B 94, 2141111 (2016).
11. A. Bhatnagar, A. R. Chaudhuri, Y. H. Kim, D. Hesse, M. Alexe, Role of domain walls in the abnormal photovoltaic effect in $BiFeO_3$. Nat. Commun. 4, 2835 (2013).
12. M.-M. Yang, A. Bhatnagar, Z.-D. Luo, M. Alexe, Enhancement of local photovoltaic current at ferroelectric domain walls in $BiFeO_3$. Sci. Rep. 7, 43070 (2017).
13. A. Zenkevich, Y. Matveyev, K. Maksimova, R. Gaynutdinov, A. Tolstikhina, V. Fridkin, Giant bulk photovoltaic effect in thin ferroelectric $BaTiO_3$ films. Phys. Rev. B 90, 161409 (2014).
14. R. Inoue, S. Takahashi, Y. Kitanaka, T. Oguchi, Y. Noguchi, M. Miyayama, Enhanced photovoltaic currents in strained Fe-doped $LiNbO_3$ films. Phys. Status Solidi A 212, 2968–2974 (2015).
15. M.-M. Yang, D. J. Kim, M. Alexe, Flexo-photovoltaic effect. Science 360, 904–907 (2018).
16. A. K. Tagantsev, Piezoelectricity and flexoelectricity in crystalline dielectrics. Phys. Rev. B 34, 5883–5889 (1986).
17. Z. L. Wang, Progress in piezotronics and piezo-phototronics. Adv. Mater. 24, 4632–4646 (2012).
18. K. Buse, Light-induced charge transport processes in photorefractive crystals II: Materials. Appl. Phys. B 64, 391–407 (1997).
19. M. Dawber, K. M. Rabe, J. F. Scott, Physics of thin-film ferroelectric oxides. Rev. Mod. Phys. 77, 1083–1130 (2005).
20. Z. Gu, D. Imbrenda, A. L. Bennett-Jackson, M. Falmbigl, A. Podpirka, T. C. Parker, D. Shreiber, M. P. Ivill, V. M. Fridkin, J. E. Spanier, Mesoscopic free path of nonthermalized photogenerated carriers in a ferroelectric insulator. Phys. Rev. Lett. 118, 096601 (2017).
21. O. F. Schirmer, M. Imlau, C. Merschejann, Bulk photovoltaic effect of $LiNbO_3$:Fe and its small-polaron-based microscopic interpretation. Phys. Rev. B 83, 165106 (2011).
22. S. I. Karabekian, S. G. Odoulov, Bulk photovoltaic effect in $LiTaO_3$:Fe crystals. Phys. Status Solidi B 169, 529–535 (1992).
23. V. M. Fridkin, Bulk photovoltaic effect in noncentrosymmetric crystals. Crystallogr. Rep. 46, 654–658 (2001).

24. V. M. Fradkin, R. M. Magomadov, Anomalous photovoltaic effect in LiNbO$_3$:Fe in polarized light. *JETP Lett.* **30**, 686–688 (1979).

25. H. G. Festl, P. Hertel, E. Krätzig, R. von Baltz, Investigations of the photovoltaic tensor in doped LiNbO$_3$. *Phys. Stat. Solidi B* **113**, 157–164 (1982).

26. Y. Zhang, Y. Liu, Z. L. Wang, Fundamental theory of piezotronics. *Adv. Mater.* **23**, 3004–3013 (2011).

27. M. Mitra, J. Drayton, M. L. C. Cooray, V. G. Karpov, D. Shvydka, Piezo-photovoltaic coupling in CdS-based thin-film photovoltaics. *J. Appl. Phys.* **102**, 034505 (2007).

28. Y. Zheng, C. H. Woo, Hyper-sensitive piezophotovoltaic effects in ferroelectric nanocylinders. *J. Appl. Phys.* **107**, 104120 (2010).

29. I. G. Austin, N. F. Mott, Polarons in crystalline and non-crystalline materials. *Adv. Phys.* **18**, 41–102 (1969).

30. O. F. Schirmer, M. Imlau, C. Merschjann, B. Schoke, Electron small polarons and bipolarons in LiNbO$_3$. *J. Phys. Condens. Matter* **21**, 123201 (2009).

31. B. Faust, H. Müller, O. F. Schirmer, Free small polarons in LiNbO$_3$. *Ferroelectrics* **153**, 297–302 (1994).

32. S. M. Young, F. Zheng, A. M. Rappe, First-principles materials design of high-performing bulk photovoltaics with the LiNbO$_3$ structure. *Phys. Rev. Appl.* **4**, 054004 (2015).

Citation: S. Nadupalli, J. Kreisel, T. Granzow, Increasing bulk photovoltaic current by strain tuning. *Sci. Adv.* **5**, eaau9199 (2019).

Science Advances

Increasing bulk photovoltaic current by strain tuning

Shankari Nadupalli, Jens Kreisel and Torsten Granzow

ARTICLE TOOLS	http://advances.sciencemag.org/content/5/3/eaau9199
SUPPLEMENTARY MATERIALS	http://advances.sciencemag.org/content/suppl/2019/02/25/5.3.eaau9199.DC1
REFERENCES	This article cites 32 articles, 1 of which you can access for free http://advances.sciencemag.org/content/5/3/eaau9199#BIBL
PERMISSIONS	http://www.sciencemag.org/help/reprints-and-permissions

Use of this article is subject to the Terms of Service